DOI: 10.1002/cbdv.202001037

FULL PAPER

CHEMISTRY & BIODIVERSITY

Induction of Apoptosis in Hepatocellular Carcinoma Cell Lines by Novel Indolylacrylamide Derivatives: Synthesis and Biological Evaluation

Mohammed Hawash,[a,1,2] Deniz Cansen Kahraman,[b,1] Rengul Cetin-Atalay,[b] and Sultan Nacak Baytas*[a]

[a] Department of Pharmaceutical Chemistry, Faculty of Pharmacy, Gazi University, 06330 Ankara, Turkey, e-mail: baytas@gazi.edu.tr

[b] Cancer Systems Biology Laboratory, Graduate School of Informatics, METU, 06800 Ankara, Turkey

Hepatocellular carcinoma (HCC) is the most prevalent primary liver cancer and one of the leading causes of cancer associated death worldwide. This is due to the highly resistant nature of this malignancy and the lack of effective treatment options for advanced stage HCC patients. The hyperactivity of PI3K/Akt and Ras/Raf/MEK/ERK signaling pathways contribute to the cancer progression, survival, motility, and resistance mechanisms, and the interaction of these two pathways are responsible for the regulation of cancer cell growth and development. Therefore, it is vital to design and develop novel therapeutic options for HCC treatment targeting these hyperactive pathways. For this purpose, novel series of *trans*-indole-3-ylacrylamide derivatives originated from the lead compound, 3-(1*H*-indole-3-yl)-*N*-(3,4,5-trimethoxyphenyl)acrylamide, have been synthesized and analyzed for their bioactivity on cancer cells along with the lead compound. Based on the initial screening, the most potent compounds were selected to elucidate their effects on cellular signaling activity of HCC cell lines. Cell cycle analysis, immunofluorescence, and Western blot analysis revealed that lead compound and (*E*)-*N*-(4-*tert*-butylphenyl)-3-(1*H*-indole-3-yl)acrylamide induced cell cycle arrest at the G2/M phase, enhanced chromatin condensation and PARP-cleavage, addressing induction of apoptotic cell death. Additionally, these compounds decreased the activity of ERK signaling pathway, where phosphorylated ERK1/2 and c-Jun protein levels diminished significantly. Relevant to these findings, the lead compound was able to inhibit tubulin polymerization as well. To conclude, the novel *trans*-indole-3-ylacrylamide derivatives inhibit one of the critical pathways associated with HCC which results in cell cycle arrest and apoptosis in HCC cell lines.

Keywords: *trans*-indole-3-ylacrylamide derivatives, cancer, hepatocellular carcinoma, apoptosis, ERK signaling pathway.

Introduction

Hepatocellular carcinoma (HCC), with about 900,000 new cases each year is the sixth most common type of cancer worldwide. The 5 year survival rate of HCC patients is only 7%.[1] Chronic infections with hepatitis B virus (HBV) or hepatitis C virus (HCV), aflatoxin exposure, chronic alcohol intake and obesity are among the risk factors associated with HCC.[2,3] Liver cancer cells are prone to acquire resistance to conventional chemotherapy and radiotherapy. Early cases usually undergo liver transplantation if available. However, when transplantation is not an option, or in advanced HCC cases, sorafenib is used as a targeted therapeutic agent. Sorafenib and Regorafenib are multikinase inhibitors approved by the Food and Drug Administration (FDA), and these drugs have both

[1] Authors contributed equally to this work.

[2] Present address: Department of Pharmacy, Faculty of Medicine and Health Sciences, An-Najah National University, Nablus, Palestine.

Supporting information for this article is available on the WWW under https://doi.org/10.1002/cbdv.202001037

antiproliferative and anti-angiogenic effects on liver cancer cells. Nevertheless, they only prolong patient survival for about 3–4 months.[4]

Mitogen-activated protein kinase (MAPK) pathways carry extracellular signals to the nucleus, and these pathways are involved in important cellular processes, including growth, proliferation, differentiation, migration, and apoptosis. The ERK pathway, which is a well-known member of MAPK pathways, is known to be deregulated in many human cancers. It is well-known that both PI3 K/Akt and Ras/Raf/MEK/ERK signaling pathways play significant roles in the development and drug resistance of HCC.[5] Hyper activation of the components of these pathways is associated with poor prognosis.[6] Therefore, development of novel drugs targeting the components of these pathways is highly critical for the treatment of patients with advanced HCC. ERK signaling pathway is also an important player for the mitotic progression of cancer cells,[7,8] and is associated with the kinetochore of mitotic spindles.[9–11] Previous studies have shown that microtubule inhibitors cause inactivation of the ERK pathway proteins and its downstream targets.[12–14] Recent studies that involve gene expression profiling emphasize that microtubule-related cellular assembly and organization is one of the most critical events in HCC development,[15–18] which makes microtubules a potential target for the therapy of HCC. Tubulin binding agents, also called 'spindle poisons', induce dysregulation of the cell cycle, characteristically at the G2/M phase,[19] and they can also be used as an alternative method to synchronize mammalian cells.[20]

A group of antimitotic compounds isolated from the South African tree *Combretum caffrum* is known as Combretastatins.[21,22] Combretastatin A-4 is a well-known natural tubulin binding molecule affecting microtubule dynamics.[23] CA-4 has low water solubility and leads to the synthesis of water-soluble derivatives. Combretastatin A-4 phosphate (CA-4P, Fosbretabulin) has been investigated for the treatment of anaplastic thyroid cancer.[24] Numerous studies have been carried out on CA-4 analogs, and their antitumoral effects have been demonstrated.[25,26] In a study conducted in 2012, phase II clinical trials for the use of combretastatin A-4 phosphate (CA-4P) in ovarian, lung, and thyroid cancers were performed.[27] Recent studies have reported 90–99% tumor necrosis with controlled doses of CA-4P, and phase III clinical trials are now being conducted.[28]

Recently, a number of CA-4 analogs with potent activities have been developed. Among these analogs, indole group-containing compounds have been reported to show antiproliferative activities.[29–34] In our previous work, starting from indole-3-carboxyaldehyde **1**, we first synthesized *trans*-indole-3-ylacrylic acid **2**, then, prepared a series of *trans*-indole-3-ylacrylamides (*Scheme 1*) and determined their cytotoxic activity against five human cancer cell lines.[35] We found that the most potent derivative among these synthesized molecules, compound **3e** was an inhibitor of tubulin polymerization and inhibited the binding of [3H] colchicine to tubulin. Compound **3e** caused cell cycle arrest in HeLa and HL-60 cells and also induced apoptotic cell death by activation of caspase-3 activity. Therefore, considering the limited availability of targeted therapies in liver cancer, in continuation of our previous work, we synthesized novel *trans*-indole-3-ylacrylamide derivatives (**4a**–**4u**, **5a**–**5s**) and evaluated their bioactivity properties on HCC cell lines and compared them to the lead compound **3e** and its analogs. The compounds were also evaluated for their effects on the cell cycle, apoptosis and ERK signaling.

Results and Discussion

Chemistry

A series of amide derivatives of *trans*-indole-3-ylacrylic acid were synthesized as illustrated in *Scheme 1*. Briefly, indole-3-carbaldehyde was condensed with malonic acid in the presence of piperidine to generate *trans*-indole-3-ylacrylic acid **2** by Knoevenagel conditions, as reported previously.[36] Amide derivatives of *trans*-indole-3-ylacrylic acid were synthesized with appropriate amines, mostly in the presence of EDC and DMAP in CH_2Cl_2. Some of the final amide derivatives (**4f**, **4g**, **4h**, **4i**, **4k**, **4m**, and **4n**) were prepared in the presence of triethylamine and ethyl chloroformate, which was used as the carboxylate activator. Compounds were purified by automated flash chromatography and checked for purity with TLC and UPLC before being tested in biological assays (purity was $>97\%$). The structures of these compounds were confirmed by FT-IR, high resolution mass spectrometry (HR-MS), ^{1}H- and ^{13}C-NMR spectral data. In the ^{1}H-NMR spectra of compounds **4a**–**4u** and **5a**–**5s**, one of the olefinic protons (C*H*=CH–CO) was observed as a doublet at about 7.56–8.02 ppm, while the other (CH=C*H*–CO) was observed as a doublet at about 6.41–6.99 ppm, with coupling constants of 15.6 or 16.0, indicating the presence of the (*E*) isomer. The more unshielded olefinic carbons (*C*H=CH–CO) were observed 167.59–165.03 ppm, the other ones (CH=*C*H–CO) were observed 125.58–125.20 ppm. The

carbonyl carbons were shifted 167.59–165.03 ppm. The synthetic procedure and spectral data of the compounds (**3a**–**3k**) were reported previously by our research group.[35]

Cytotoxicity of trans-Indole-3-ylacrylamide Derivatives on Cancer Cells and HCC Cell Lines

trans-Indole-3-ylacrylamide derivatives **3a**–**3k**, **4a**–**4u**, and **5a**–**5s** were primarily screened against hepatocellular (Huh7), breast (MCF7) and colon carcinoma (HCT116) cells using the Sulforhodamine B (SRB) assay.[37] IC_{50} values of compounds were between 0.5–40.6 μM and were compared to those of the well-known chemotherapeutic agents, doxorubicin (DOXO) and 5-fluorouracil (5-FU) as well as multikinase inhibitor Sorafenib (*Table 1*).

When the results of the initial screening experiments were examined, the R^1 moiety in the *trans*-indole-3-ylacrylamide structure had a considerable impact on cytotoxicity. In the amide section, the phenyl ring directly attached to the amide nitrogen was found to be required for activity. Activity was observed in the polymethoxyphenyl bearing derivatives (**3a**–**3f**) at the amide site, while cell growth inhibitory activity was lost in the polymethoxybenzyl derivatives (**3g**–**3j**). Compound **4a** from polymethoxybenzyl amide derivatives inhibited cell growth in Huh7 cells with an IC_{50} value of 9.3 μM. Compound **4a** carries a 3,4,5-trimethoxybenzyl group similar to the precursor compound **3e** bearing the 3,4,5-trimeth-

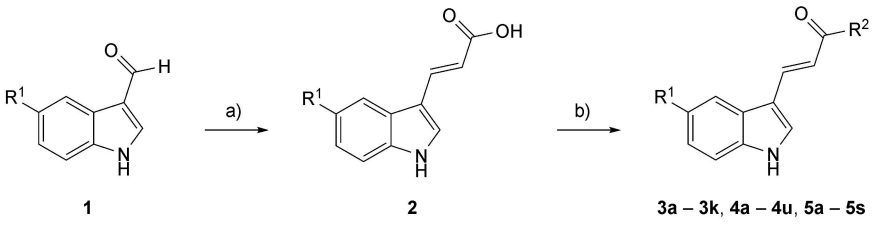

1 **2** **3a – 3k, 4a – 4u, 5a – 5s**

R^1 = H for **3a – 3k**, **4a – 4u**, **5a – 5o**
R^1 = Br for **5p – 5s**

R^2 =

3a, *N*-(2,4-dimethoxyphenyl)
3b, *N*-(2,5-dimethoxyphenyl)
3c, *N*-(3,4-dimethoxyphenyl)
3d, *N*-(3,5-dimethoxyphenyl)
3e, *N*-(3,4,5-trimethoxyphenyl)
3f, *N*-(2,4,6-trimethoxyphenyl)
3g, *N*-(4-hydroxy-3-methoxybenzyl)
3h, *N*-(2,3-dimethoxybenzyl)
3i, *N*-(2,4-dimethoxybenzyl)
3j, *N*-(2,5-dimethoxybenzyl)
3k, *N*-(3,4-dimethoxybenzyl)

4a, *N*-(3,4,5-trimethoxybenzyl)
4b, *N*-(4-methoxybenzyl)
4c, *N*-benzyl
4d, *N*-(4-(methylthio)phenyl)
4e, *N*-(4-chlorophenyl)
4f, *N*-(2-chlorophenyl)
4g, *N*-(3-chlorophenyl)
4h, *N*-(2-chlorobenzyl)
4i, *N*-(2,4-dichlorophenyl)
4j, *N*-(4-bromophenyl)
4k, *N*-(2,6-dimethylphenyl)
4l, *N*-(4-(*tert*-butyl)phenyl)
4m, piperidin-1-yl
4n, morfolino
4o, 2-(ethoxycarbonyl)-piperidin-1-yl
4p, *N*-cyclohexyl
4r, *N*-(4-methylcyclohexyl)
4s, *N*-(1-benzylpiperidin-4-yl)
4t, *N*-butyl
4u, *N*-(3-(2-methyl-1 *H*-imidazole-1-yl)propyl)

5a, *N*-(pyridin-2-ylmethyl)
5b, *N*-(pyridin-3-ylmethyl)
5c, *N*-(pyridin-4-ylmethyl)
5d, *N*-(2-(pyridin-2-yl)ethyl)
5e, *N*-(2-(pyridin-3-yl)ethyl)
5f, *N*-(2-(pyridin-4-yl)ethyl)
5g, *N*-phenethyl
5h, 4-(2-ethoxyethyl)piperazin-1-yl
5i, 4-(pyridin-4-yl)piperazin-1-yl
5j, 4-(pyridin-2-yl)piperazin-1-yl
5k, 4-(4-chlorophenyl)piperazin-1-yl
5l, 4-(4-fluorophenyl)piperazin-1-yl
5m, 4-(4-methoxyphenyl)piperazin-1-yl
5n, 4-(*p*-tolyl)piperazin-1-yl
5o, *N*-(4-methoxyphenyl)
5p, *N*-(3,4,5-trimethoxyphenyl)
5r, *N*-(3,4,5-trimethoxybenzyl)
5s, *N*-(4-(*tert*-butyl)phenyl)

Scheme 1. Synthesis pathway to achieve the title compounds. Reagents and conditions: a) Malonic acid, piperidine, pyridine, 5 h, 40 °C; b) *i.* amine derivative, EDC, DMAP, CH_2Cl_2, overnight, r.t. or *ii.* amine derivative, ethyl chloroformate, Et_3N, CH_2Cl_2, overnight, r.t.

Table 1. IC_{50} values of *trans*-indole-3-ylacrylamide derivatives on Huh7, MCF7 and HCT116 cancer cells.

Compound	IC_{50} (μM)[a]		
	Huh7	MCF7[b]	HCT116
3a	34.5 ± 6.0	–	NI
3b	21.2 ± 2.9	–	28.0 ± 5.7
3c	23.5 ± 3.2	–	NI
3d	17.1 ± 1.9	–	24.0 ± 0.7
3e	0.5 ± 0.2	–	1.1 ± 0.7
3f	NI	–	NI
3g	NI	–	NI
3h	20.9 ± 2.4	–	NI
3i	NI	–	NI
3j	NI	–	NI
3k	NI	–	NI
4a	9.3 ± 1.7	NI	26.7 ± 4.2
4b	33.1 ± 9.9	NI	NI
4c	NI	NI	NI
4d	7.9 ± 0.2	8.3 ± 1.0	16.6 ± 1.4
4e	11.7 ± 0.3	12.1 ± 1.0	19.6 ± 1.2
4f	11.7 ± 4.6	25.4 ± 4.5	26.4 ± 1.9
4g	10.8 ± 2.2	13.1 ± 1.0	12.7 ± 0.2
4h	12.8 ± 3.5	40.6 ± 3.4	29.0 ± 1.5
4i	13.2 ± 1.7	15.1 ± 1.2	18.3 ± 3.5
4j	11.7 ± 0.6	14.9 ± 1.9	20.4 ± 3.7
4k	31.4 ± 5.8	NI	NI
4l	3.1 ± 1.7	2.0 ± 0.4	5.7 ± 1.4
4m	NI	NI	NI
4n	NI	NI	NI
4o	16.0 ± 1.7	NI	NI
4p	18.2 ± 4.7	NI	NI
4r	24.1 ± 5.8	38.3 ± 1.3	36.3 ± 5.8
4s	34.3 ± 14.5	NI	NI
4t	32.2 ± 4.6	NI	NI
4u	NI	NI	NI
5a	NI	NI	NI
5b	NI	NI	NI
5c	NI	NI	NI
5d	NI	NI	NI
5e	NI	NI	NI
5f	NI	NI	NI
5g	10.7 ± 2.8	18.9 ± 2.3	24.2 ± 3.1
5h	NI	NI	NI
5i	NI	26.9 ± 4.6	Nİ
5j	30.1 ± 5.1	NI	NI
5k	22.4 ± 4.6	18.7 ± 3.6	24.0 ± 2.7
5l	18.3 ± 1.3	28.7 ± 4.4	22.1 ± 2.1
5m	24.0 ± 3.5	NI	NI
5n	29.2 ± 2.3	NI	NI
5o	19.6 ± 0.1	ND	ND
5p	4.9 ± 0.5	ND	ND
5r	18.0 ± 1.5	ND	ND
5s	4.3 ± 0.5	ND	ND
DOX	0.22 ± 0.02	0.14 ± 0.05	0.23 ± 0.02
5-FU	2.0 ± 0.04	1.5 ± 0.1	1.3 ± 0.2
Sorafenib	6.5 ± 0.5	14.6 ± 0.2	11 ± 0.6

[a] Data was represented as the mean ± SD, $n = 3$. [b] IC_{50} values for compound **3a**–**3k** in MCF7 cell lines could be found in our previously published study,[35] NI: No inhibition; ND: Not determined.

oxyphenyl group in the amide moiety. These results show that the structure of 3,4,5-trimethoxyphenyl directly bonded to amide nitrogen is important for its activity. Compound **4l**, bearing a *tert*-butyl group at position 4 of the phenyl ring attached to the amide nitrogen, showed significant activity against the three cell lines (IC_{50} Huh7, 3.1 μM; MCF7, 2.0 μM; and HCT116; 5.7 μM). Compound **4l** is the compound with activity closest to that of the lead compound **3e** among the synthesized compounds. Compound **4d**, carrying a 4-thiomethylphenyl group attached to the amide nitrogen, also showed activity against the three cell lines (IC_{50} Huh7, 7.9 μM; MCF7, 8.3 μM, and HCT116, 16.6 μM). Weaker activity was observed in the halogen substituted phenyl derivatives (**4e**–**4j**) bound to the amide nitrogen, with IC_{50} values above 10 μM (IC_{50} 10.8–40.6 μM). A considerable decrease in activity was observed with a methyl substitution in the phenyl ring attached to the amide nitrogen (**4k**, IC_{50} 31.4 μM). When a benzyl group was attached to the amide nitrogen, activity disappeared (**4c**). The methoxy group placed in the 4 position of the benzyl group resulted in low activity in the Huh7 cell lines (**4b**, IC_{50} 33.1 μM). When saturated, nitrogen containing, cyclic rings replaced the amide nitrogen (**4m**, **4n**, **4s**), activity was greatly reduced or disappeared. Compounds carrying imidazole and pyridine rings linked by an aliphatic intermediate chain in the amide moiety were also synthesized, but activity was lost in these compounds (**4u**–**5f**). Altogether, important data about structure-activity relationships were obtained from these *trans*-indole-3-ylacrylamide derivatives. For cytotoxic activity, in the amide portion of the *trans*-indole-3-ylacrylamide derivatives, there is a requirement for a phenyl ring directly linked to the amide nitrogen and substituted with a bulky group.

Moreover, the IC_{50} values of selected compounds (**3e**, **4d**, **4l**, **5p**, and **5s**) were comparable to those of doxorubicin and sorafenib, which are agents, used clinically for HCC conventional chemotherapy and targeted therapy. These compounds were therefore, chosen to be tested in a panel of HCC cells (Huh7, HepG2, Mahlavu and SNU475). The inhibitory concentrations of the selected compounds were determined using SRB assay and listed in *Table 2*.

The results have shown that compound **3e** had IC_{50} values of 1 μM or less in the two more aggressive HCC cell lines, Mahlavu and SNU475. Similarly, compound **4l**, which exhibited the closest activity to the lead compound **3e** among the synthesized compounds, showed strong inhibition of the growth of both Mahlavu and SNU475 cells.

Table 2. IC_{50} values (μM) determined in a liver cancer cell panel for compounds **3e**, **4d**, **4l**, **5p** and **5s**.

Compound	IC_{50} (μM)[a]			
	Huh7	HepG2	Mahlavu	SNU475
3e	0.5 ± 0.2	3.6 ± 0.6	1.0 ± 0.1	0.3 ± 0.1
4d	7.9 ± 0.2	11.5 ± 0.8	12.2 ± 0.8	25.3 ± 1.1
4l	3.1 ± 1.7	4.8 ± 0.8	5.3 ± 0.5	8.4 ± 1.0
5p	4.9 ± 0.5	> 40	32.0 ± 0.3	7.6 ± 0.5
5s	4.3 ± 0.5	11.5 ± 1.1	6.6 ± 1.8	10.7 ± 0.7

[a] Data was represented as the mean ± SD, $n = 3$.

Considering our previous work where our lead compound **3e** was an inhibitor of tubulin polymerization and inhibited the binding of [^{3}H]colchicine to tubulin,[35] we investigated the tubulin polymerization inhibition and colchicine binding capacity of the compounds **4d**, **4l**, **5p**, and **5s**. We determined that the compounds were inactive as anti-tubulin agents (data not shown). Furthermore, when all the selected compounds (**3e**, **4d** and **4l**) were screened against normal human epithelial breast cell lines, MCF12A, all had relatively higher IC_{50} values (between 17.8–36.1 μM) (*Table S2*), indicating selective bioactivities of these compounds towards cancer cells.

Real-Time Cell Growth Monitoring of HCC Cells Treated with 3e, 4d***, and*** 4l

The effects of the compounds on growth of HCC cells were evaluated using real-time cell electronic sensing system (RT-CES). The growth patterns of all cells suggested that all compounds were able to decrease the growth rate in a dose dependent manner (*Figure 1*). In addition, the growth pattern of the HCC cells led to the hypothesis that these compounds caused an arrest in the cell cycle, where cells neither grow in number nor die completely after a 72 h treatment.[38] In contrast, DMSO treated control cells were able to proliferate at their normal pace.

Apoptotic Cell Death Induced by the Selected Indole-3-ylacrylamide Derivatives 3e, 4d***, and*** 4l

For the evaluation of induction of cell death by indole-3-ylacrylamide derivatives **3e**, **4d**, and **4l**, HCC cells were treated with the compounds for 48 h, and their nuclei were stained and analyzed under fluorescent microscopy. Condensed chromatin structure as well as nuclear blebbings were visible in all cells treated with compounds (*Figure 2a*), the effect observed with **3e** being the greatest. Furthermore, the apoptotic marker, cleaved PARP, was observed in both well-differentiated (Huh7 and HepG2) and poorly differentiated (Mahlavu and SNU475) cells,[39] after a 24 h treatment (*Figure 2b*) confirming that apoptotic cell death was induced by these compounds.

G2/M Arrest Induced by the Selected trans-Indole-3-ylacrylamide Derivatives 3e, 4d ***and*** 4l

Because of the growth pattern of cells obtained in the real-time cell growth assay, flow cytometry analysis was performed by staining DNA with propidium iodide (PI). Our goal was to determine if the indole-3-ylacrylamide derivatives altered the progression of the cell cycle at a certain stage. After 48 h treatment, compound **3e** caused G2/M arrest substantially in all four cell lines. Compound **4l** caused a minor change in the percentage of cells in G2/M phase, especially in mesenchymal-like cells (Mahlavu and SNU475). Compound **4d** did not cause any considerable change in cell cycle distribution, except for a small increase in G2/M cells in the Mahlavu cells at 24 and 48 h (*Figure 3*).

Effects of trans-Indole-3-ylacrylamide Derivatives 3e, 4d***, and*** 4l ***on Akt, ERK and c-Jun***

An epithelial-like cell lines, Huh7 and a mesenchymal-like cell lines Mahlavu (with hyperactive Akt pathway due to PTEN loss[40]) were chosen for further analysis of the Akt and ERK pathway, which are associated with the development of HCC and poor prognosis in patients as mentioned previously. Western blot analysis revealed that the compounds had no significant effect on the levels of active form of (Ser473 phosphorylated) Akt protein whereas, all the selected compounds were able to decrease levels of the activated form of (Thy204 phosphorylated) ERK1/2 protein. Compound **3e** and **4d** were able to reduce the levels of c-Jun proteins as well in both Huh7 and

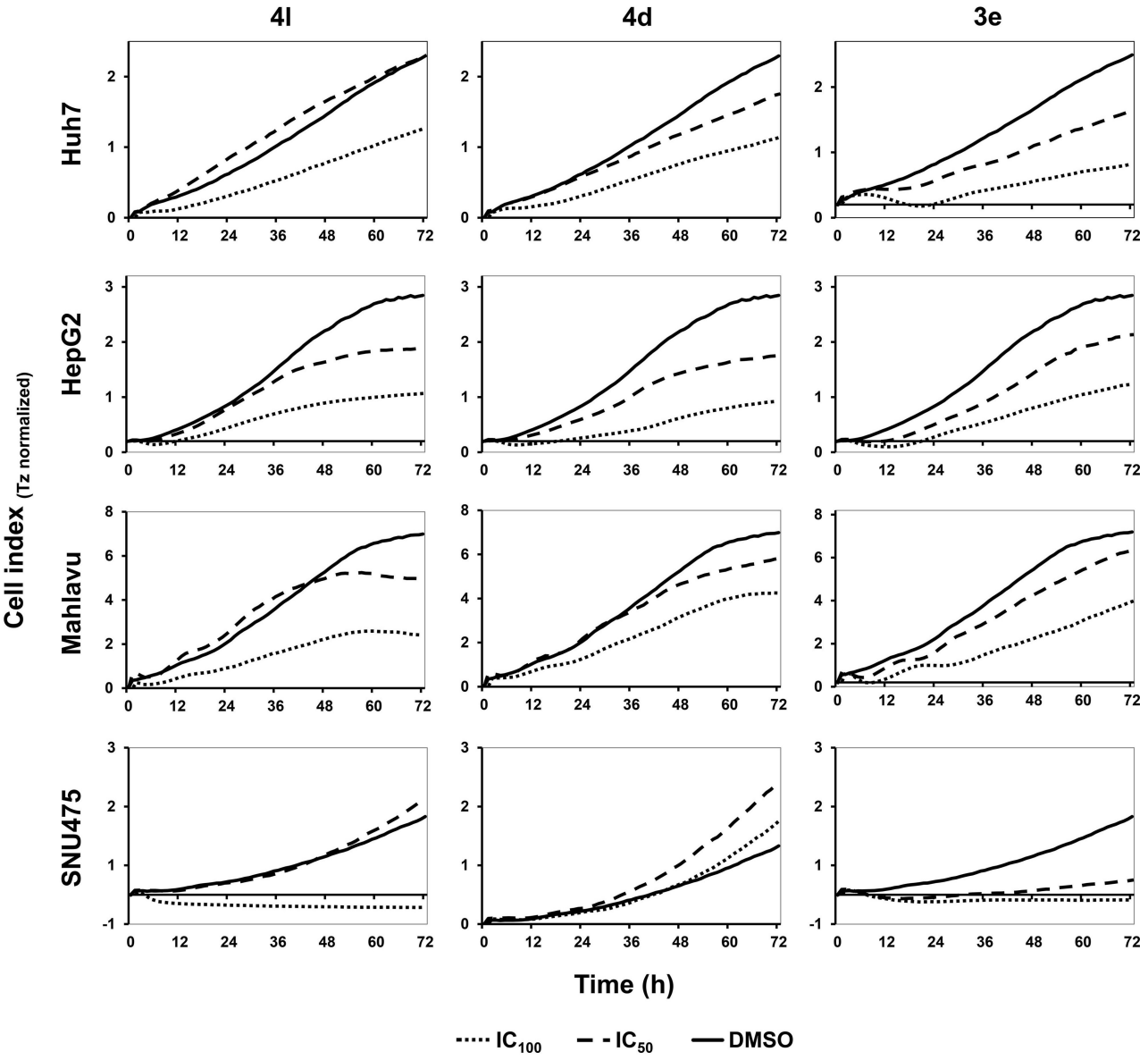

Figure 1. Real-time cell monitoring of HCC cell lines treated with compounds **3e**, **4d**, and **4l** at IC_{50} and IC_{100} concentrations for 72 h. Growth of treated cells was compared to that of a DMSO control (0.1 %).

Mahlavu cells (*Figure 4*). Thus, indole-3-ylacrylamide derivatives able to hinder the activity of ERK protein and its downstream targets such as c-Jun these effects were independent of the Akt pathway activity (phospho-Akt^{Ser473}), which also controls c-Jun. This analysis indicates that the compounds are specifically effective on the ERK protein.

Conclusions

With regard to our previous knowledge about our lead compound, which exhibits anti-microtubule activity and induces apoptosis, we aimed to expand our work with the newly synthesized trans-indole-3-ylacrylamide derivatives. For this purpose, a new series of trans-indole-3-ylacrylamide derivatives were synthesized, and their bioactivities were evaluated in different cancer cell lines (HCC, breast, and colon carcinoma). The cytotoxic bioactivities of the compounds were

compared with those of the clinically used chemotherapeutic agents, doxorubicin, and 5-FU as well as the multikinase inhibitor sorafenib. Our results have revealed that trans-indole-3-ylacrylamides induce G2/M arrest (*Figure 3*) and apoptotic cell death as demonstrated with nuclear Hoechst staining and the PARP cleavage. Western blot analysis has showed that, compounds **3e** and **4d** reduced the levels of activated ERK and its downstream signaling element c-Jun protein. As mentioned previously, since ERK signaling and cell cycle arrest characteristically at the G2/M phase is associated with inhibition of tubulin polymer-

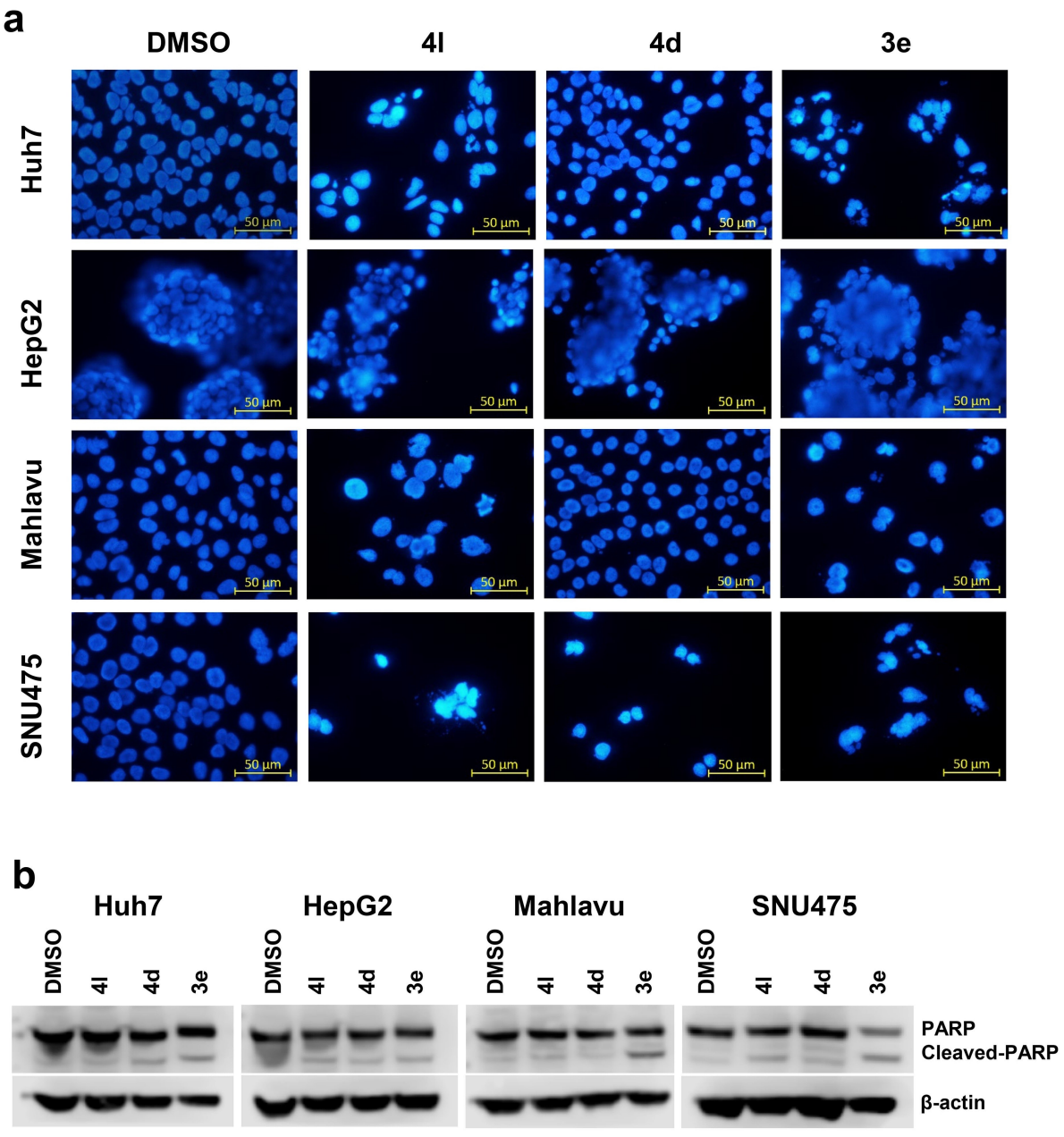

Figure 2. Induction of apoptosis in HCC cell lines treated with selected compounds. a) Images of Nuclear Hoechst 33258 staining after incubation of cells with IC_{50} concentrations of compounds **4l**, **4d** or **3e** for 48 h taken at a 20× magnification; b) Western blot analysis of cleaved PARP levels in well-differentiated (Huh7 and HepG2) and poorly differentiated (Mahlavu and SNU475) HCC cells treated with the corresponding IC_{100} concentrations of the same compounds for 24 h.

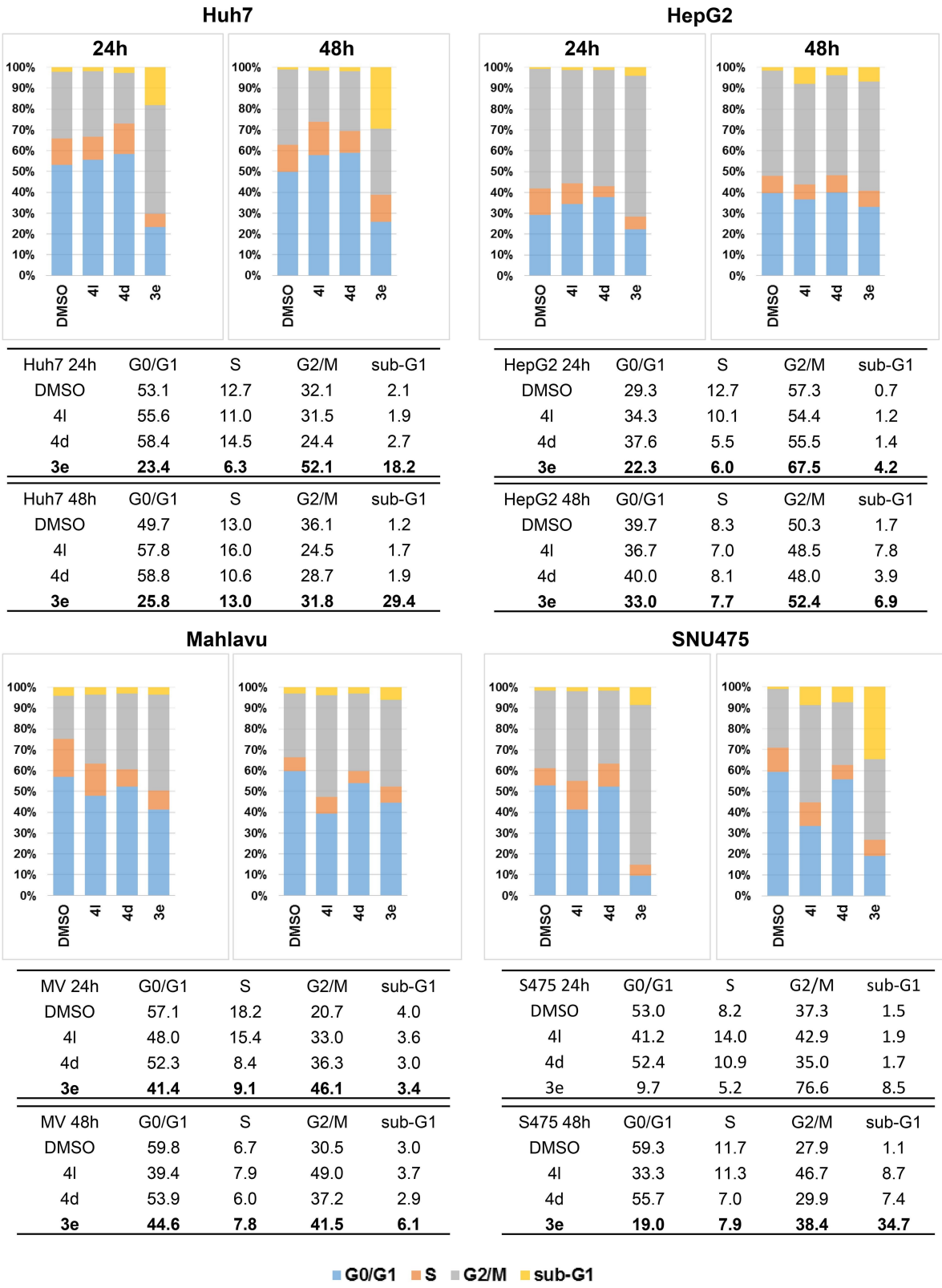

Huh7 24h	G0/G1	S	G2/M	sub-G1
DMSO	53.1	12.7	32.1	2.1
4l	55.6	11.0	31.5	1.9
4d	58.4	14.5	24.4	2.7
3e	**23.4**	**6.3**	**52.1**	**18.2**

Huh7 48h	G0/G1	S	G2/M	sub-G1
DMSO	49.7	13.0	36.1	1.2
4l	57.8	16.0	24.5	1.7
4d	58.8	10.6	28.7	1.9
3e	**25.8**	**13.0**	**31.8**	**29.4**

HepG2 24h	G0/G1	S	G2/M	sub-G1
DMSO	29.3	12.7	57.3	0.7
4l	34.3	10.1	54.4	1.2
4d	37.6	5.5	55.5	1.4
3e	**22.3**	**6.0**	**67.5**	**4.2**

HepG2 48h	G0/G1	S	G2/M	sub-G1
DMSO	39.7	8.3	50.3	1.7
4l	36.7	7.0	48.5	7.8
4d	40.0	8.1	48.0	3.9
3e	**33.0**	**7.7**	**52.4**	**6.9**

MV 24h	G0/G1	S	G2/M	sub-G1
DMSO	57.1	18.2	20.7	4.0
4l	48.0	15.4	33.0	3.6
4d	52.3	8.4	36.3	3.0
3e	**41.4**	**9.1**	**46.1**	**3.4**

MV 48h	G0/G1	S	G2/M	sub-G1
DMSO	59.8	6.7	30.5	3.0
4l	39.4	7.9	49.0	3.7
4d	53.9	6.0	37.2	2.9
3e	**44.6**	**7.8**	**41.5**	**6.1**

S475 24h	G0/G1	S	G2/M	sub-G1
DMSO	53.0	8.2	37.3	1.5
4l	41.2	14.0	42.9	1.9
4d	52.4	10.9	35.0	1.7
3e	9.7	5.2	76.6	8.5

S475 48h	G0/G1	S	G2/M	sub-G1
DMSO	59.3	11.7	27.9	1.1
4l	33.3	11.3	46.7	8.7
4d	55.7	7.0	29.9	7.4
3e	**19.0**	**7.9**	**38.4**	**34.7**

Figure 3. Cell cycle analysis of HCC cell lines Huh7, HepG2, Mahlavu (MV), and SNU475 (S475) treated with the IC_{100} concentrations of compounds **3e**, **4d**, and **4l** for 24 and 48 h. Bar graphs indicate the overall cell cycle distribution; tables present corresponding values at indicated times for each cell lines.

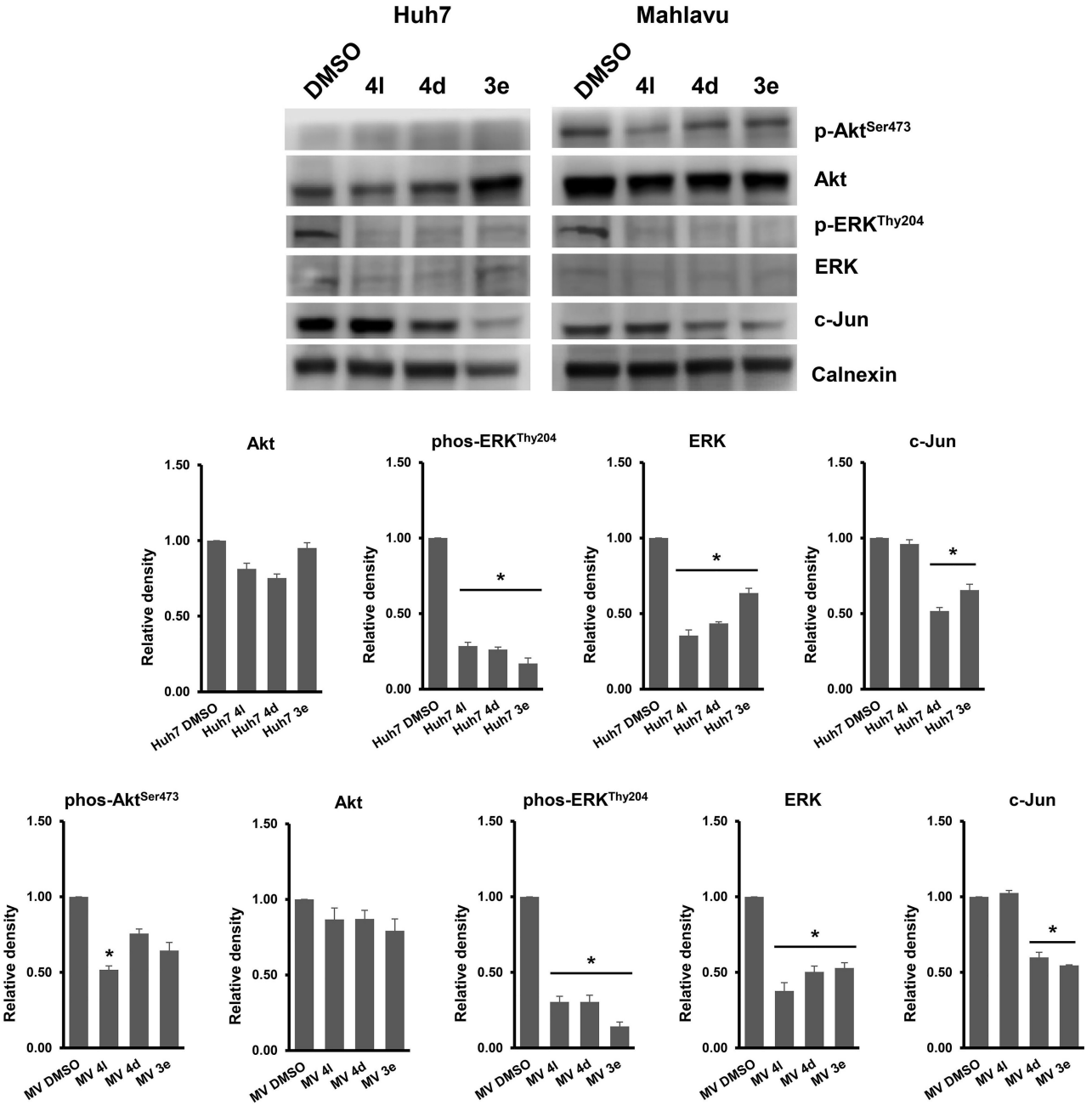

Figure 4. Representative images of Western blot analysis of Akt, ERK, and c-Jun proteins following treatment of the indicated cell lines with **3e**, **4d** and **4l** for 24 h at the IC_{100} concentrations. Phosphorylation of Akt (Ser473) is indicative of the levels of active Akt, and phosphorylation of ERK (Thr204) results in its activation. c-Jun is a downstream protein of both the ERK and Akt pathways. Calnexin was used as a loading control. Bar graphs indicate relative band intensities of treatments with respect to DMSO control groups for each cell lines. Bar graphs indicate statistical analysis of band intensities of treatments with respect to DMSO control groups for each cell lines from $n = 3$ experiments (values are represented as mean $\pm$ SD). Statistical analysis was performed using a Student's t-test, $^*P < 0.05$.

ization, our results with compound **3e** further supported the hypothesis that compound **3e** acts as a microtubule targeting agent, whereas compounds **4d** and **4l** were found to act on the ERK signaling pathway, independent of mechanisms involved in tubulin polymerization (*Figure 4*). In addition, the lack of any alteration in Akt protein phosphorylation (activation) in the presence of the compounds, demonstrated that the molecular action primarily of **3e** as well as **4d** and **4l** involve the ERK protein.

To conclude, this study has provided valuable information on the potential of compound **3e** and newly synthesized trans-indole-3-ylacrylamide derivatives **4d** and **4l** to inhibit the ERK pathway, one of the critical pathways involved in HCC occurrence, and induce cell cycle arrest and apoptotic cell death in HCC cell lines. Yet, additional information about the molecular targets of these compounds remains to be investigated through biochemical and computational target identification approaches.

Experimental Section

Chemistry

Melting points were determined with an SMP-II Digital Melting Point Apparatus and are uncorrected (Schorpp Geaetetechnik, Germany). IR spectra were obtained using a Perkin Elmer Spectrum 400 FT-IR/FTNIR spectrometer equipped with a Universal ATR Sampling Accessory. ^{1}H-NMR spectra were recorded in $CDCl_3$ or (D_6)DMSO on a Varian Mercury 400 MHz High Performance Digital FT-NMR spectrometer at the NMR facility of the Faculty of Pharmacy, Ankara University, and ^{13}C-NMR spectra were recorded in (D_6)DMSO on a Bruker Avance Ultrashield 300 MHz NMR spectrometer at the NMR facility of the Faculty of Science, Gazi University using tetramethylsilane as the internal standard. All chemical shifts were recorded as δ (ppm). High resolution mass spectra data (HR-MS) were collected using a Waters LCT Premier XE Mass Spectrometer (high sensitivity orthogonal acceleration time-of-flight instrument) using the ESI (+) or ESI (−) methods. The instrument was coupled to an AQUITY Ultra Performance Liquid Chromatography system (Waters Corporation, Milford, MA, USA). Flash chromatography was performed with a Combiflash®Rf automated flash chromatography system with RediSep columns (Teledyne-Isco, Lincoln, NE, USA) using DCM/MeOH, hexane/AcOEt, and AcOEt/DCM solvent gradients.

Synthesis of trans-Indole-3-ylacrylamide Derivatives (4a–4u, 5a–5s)

Procedure 1. Amine derivatives (1.8 mmol), DMAP (0.3 mmol), and EDCI (1.65 mmol) were added in sequence to a solution of the indole acrylic acid (1.5 mmol) in CH_2Cl_2 (5 mL) and dimethylformamide (DMF) (0.5 mL) under N_2. The solution was stirred at room temperature for 24–48 h. Progress of the reaction was followed by TLC. After completion of the reaction, the solvent was evaporated under reduced pressure, the residue was dissolved in CH_2Cl_2, and the organic phase was washed with a 1% $NaHCO_3$ solution and brine, dried over Na_2SO_4, and evaporated under vacuum. The final residue was purified by flash column chromatography (Combiflash® Rf) using DCM/MeOH and hexane/ethyl acetate solvent gradients. Some derivatives were recrystallized using a different solvent system.

Procedure 2. To a solution of the acid derivative (1.5 mmol) in CH_2Cl_2 were added triethylamine (3 mmol) and ethyl chloroformate (1.5 mmol), followed by stirring at 0 °C for 30 min. After the addition of the appropriate amine derivative (1.8 mmol), the mixture was stirred for an additional 1 h at 0 °C. Then, the reaction mixture was warmed to room temperature and stirred overnight. The progress of the reaction was followed by TLC. After completion of the reaction, the solvent was evaporated under reduced pressure, the residue was dissolved in CH_2Cl_2, and the organic phase was washed with a 1% $NaHCO_3$ solution and brine, dried over Na_2SO_4, and evaporated under vacuum. The final residue was purified by flash column chromatography (Combiflash® Rf) using DCM/MeOH and hexane/ethyl acetate solvents gradients, some derivatives being recrystallized by different solvent systems.

Examples of spectra data of **4d** and **4l** are shown below, whereas data of rest of the final derivatives are listed in the *Supporting Information*.

Data for **(2*E*)-3-(1*H*-Indol-3-yl)-*N*-[4-(methylsulfanyl)phenyl]prop-2-enamide** (**4d**). Prepared using procedure 1. Purified by flash column chromatography (0%→6% methanol in CH_2Cl_2). Yield 22%. M.p. 224–225 °C. IR (FT-IR/FTNIR-ATR): 1641 cm^{-1} (C=O). ^{1}H-NMR (400 MHz, (D_6)DMSO): 11.62 (1H, s), 9.97 (1H, s), 7.94–7.92 (1H, m), 7.80 (1H, d, J=2.8), 7.73 (1H, d, J=15.6), 7.66–7.63 (2H, m), 7.46–7.44 (1H, m), 7.23 (2H, d, J=8.4), 7.20–7.16 (2H, m), 6.76

(1H, d, $J=15.6$), 2.43 (3H, s). ^{13}C-NMR (300 MHz, (D_6) DMSO): 165.37, 137.94, 137.89, 135.21, 131.64, 131.58, 127.84, 125.30, 122.83, 120.96, 120.47, 119.97, 116.34, 112.87, 112.66, 16.16. HR-MS (*m/z*): $[M+H]^+$ calc. for $C_{18}H_{17}N_2OS$ 309.1062, found 309.1060.

Data for **(2*E*)-*N*-(4-*tert*-Butylphenyl)-3-(1*H*-indol-3-yl)prop-2-enamide** (**4l**). Prepared using procedure 1. Purified by flash column chromatography (0%→ 20% methanol in CH_2Cl_2). Yield 23%. M.p. 275–276 °C. IR (FT-IR/FTNIR-ATR): 1643 cm^{-1} (C=O). ^{1}H-NMR (400 MHz, (D_6)DMSO): 11.63 (1H, s), 9.90 (1H, s), 7.96 (1H, d, $J=6.8$), 7.82 (1H, s), 7.74 (1H, d, $J=15.6$), 7.61 (2H, d, $J=6.8$), 7.47 (1H, d, $J=6.4$), 7.33 (2H, d, $J=8.4$), 7.24–7.18 (2H, m), 6.80 (1H, d, $J=15.6$), 1.27 (9H, s). ^{13}C-NMR (300 MHz, (D_6)DMSO): 165.28, 145.51, 137.93, 137.71, 134.93, 131.47, 128.88, 125.83, 125.30, 122.79, 120.91, 120.49, 119.08, 118.65, 116.60, 112.84, 112.68, 34.46, 31.60. HR-MS (*m/z*): $[M+H]^+$ calc. for $C_{21}H_{23}N_2O$ 319.1810, found 319.1797.

Biological Studies

Drugs and Chemicals

Sulforhodamine B (SRB) and Dimethyl sulfoxide (DMSO) was purchased from Sigma–Aldrich. 5-Fluorouracil (5-FU), Doxorubicin (DOXO) and Sorafenib was obtained from Calbiochem. The stock solutions (20 mM) of test compounds and drugs were prepared in DMSO and stored at −20 °C.

Cell Culture

HCC cell lines (Huh7, HepG2, and Mahlavu, human breast carcinoma cells (MCF7) and human colon carcinoma cells (HCT116) were grown in Dulbecco's Modified Eagles Medium (DMEM) supplemented with 10% fetal bovine serum (FBS) (Invitrogen, GIBCO) and 1% non-essential amino acids (Invitrogen, GIBCO). SNU475 cells were grown in RPMI-1640 media (Invitrogen, GIBCO) supplemented with 10% FBS and 2 mM L-glutamine. Normal human epithelial breast cells (MCF-12A) were grown in DMEM/HAM's F12 medium supplemented with 10% fetal bovine serum (FBS) and 1% non-essential amino acids, 10 ng/ml EGF, 500 ng/ml hydrocortisone and 10 μg/ml insulin. All media were also supplemented with 100 units/mL penicillin and streptomycin, and cells were maintained in a humidified incubator with 5% CO_2, at 37 °C. Cell lines used in this study are short tandem repeat (STR) authenticated and are regularly tested with (MycoAlert, Lonza) mycoplasma test kit for mycoplasma contamination.

Sulforhodamine B (SRB) Assay

SRB assay was performed as described previously.[41] Briefly, cells were plated in 96-well plates (1000–3000 cells/well) and grown for 24 h. Cells were treated with the compounds at different concentrations (40–2.5 μM) in triplicates. The final DMSO concentration was 0.1% in each well. After 72 h, cell fixation was done with 10% (v/v) trichloroacetic acid (MERCK) and cells were stained with SRB solution (50 μL of 0.4% (w/v) SRB in 1% acetic acid). Unbound SRB was removed by washing each well with 1% acetic acid followed by air-drying. Before absorbance measurements at 515 nm, SRB was solubilized in 10 mM Tris-base. Percent growth inhibition (% inhibition $=100\times(1-OD_{drug}/OD_{DMSO})$ vs. drug concentration values were used to generate dose-response curves to calculate IC_{50} values for each compound.

Real-Time Cell Growth Surveillance by Electronic Sensing (RT-CES)

Real-time cell growth monitoring of HCC cells was performed using the xCELLigence System (Agilent) as described previously.[41] Briefly, cells were seeded into 96-well E-plates (1000–3000 cells/well) and monitored every 30 min until the cells reached their log (growth) phase. Then, treatments with the compounds (IC_{50} and IC_{100} conc.), and with DMSO (control) were done. The cell index (CI) values were recorded every 30 min for a total of 72 h. Time-zero normalized CI values were used to demonstrate cell growth graphs for each cell lines.

Nuclear Staining with Hoechst 33258

Cells were seeded onto coverslips placed in 6-well plates. Following 24 h, cells were treated with the compounds (IC_{50} conc. for 48 h). Then, cells were fixed with 100% cold methanol for 10 min. Cells were then washed with cold 1xPBS for several times before nuclear staining. 1 μg/ml Hoechst 33258 dye was used to stain nuclei and incubated for 5 min at room temperature. De-staining was done with ddH_2O for 10 min to remove excess dye. Apoptotic nuclei were identified using a blue filter (340–380 nm) on a fluorescence microscope (Nikon Eclipse 50i).

Cell Cycle Analysis

Cells were seeded onto 10 cm culture dishes and grown for 24 h. Then, cells were treated with the compounds (IC_{100} conc.) for 24 or 48 h. Cells were fixed with ice-cold 70% ethanol at −20 °C for 3 h before propidium iodide (PI) staining. MUSE Cell Cycle Assay kit (Millipore) was used to stain cells, cell cycle distributions was determined using MUSE Cell Analyzer (Millipore) according to the manufacturer's recommendations.

Western Blot Analysis

Cells were seeded onto 15 cm culture dishes and treated with the compounds (IC_{100} conc.) or with DMSO for 24 h. Mini-PROTEAN® Tetra Cell Systems and TGX™ precast gels (loaded with 20–40 μg/well protein) were used for gel electrophoresis according to the manufacturer's instructions. Then proteins were transferred to PVDF membrane using the Trans-Blot® Turbo Transfer System (Bio-Rad). For immunoblotting, α-calnexin (Cell Signaling, 2679), α-phospho-Akt (Cell Signaling, 9271), α-Akt (Cell Signaling, 9272S), α-phospho-Erk (Santa Cruz, 16982), α-Erk (Santa Cruz, sc-135900), α-c-Jun (Santa Cruz, sc-45), α-PARP (Cell Signaling, 9532S) and β-actin (Cell Signaling, 4967) primary antibodies, followed by HRP-conjugated goat anti-mouse IgG (Sigma-Aldrich, A0168), rabbit anti-goat IgG (Sigma-Aldrich A8919), or goat anti-rabbit IgG (Sigma-Aldrich, A6154) secondary antibodies were used. Then, proteins of interest were identified using the C-Digit® imaging system (LI-COR). The intensity of the bands was quantified using ImageJ program and intensity values for each sample were normalized to that of Calnexin.

Statistical Analysis

All data in this study were acquired from $n=3$ independent experiments and are shown with calculated ±SD values accordingly. Student's t-test was performed for statistical analysis (Prism, Graphpad or Microsoft Excel) and statistical significance was represented as follows: $^*P<0.05$.

Acknowledgements

This work was supported by The Scientific and Technological Research Council of Turkey (TUBITAK, Grant# 113S973) to S.N.B. and Turkish Ministry of Development project (KanSiL_2016K121540), to R.C.A. We would like to thank Tugce Oksakli for laboratory technical assistance in KanSil.

Author Contributions Statements

S.N.B designed the compounds and their synthesis. M.H. performed the chemical synthesis and characterized the compounds. R.C.A. and D.C.K. designed the biological experiments. D.C.K. performed the experiments for biological evaluation of the compounds on HCC cell lines. S.N.B., M.H., D.C.K. and R.C.A. contributed to the writing of the manuscript. All authors have given approval to the final version of the manuscript.

References

[1] B. W. Stewart, C. Wild, 'World Cancer Report 2014', International Agency for Research on Cancer, World Health Organization, 2014.
[2] G. Baffy, E. M. Brunt, S. H. Caldwell, 'Hepatocellular carcinoma in non-alcoholic fatty liver disease: An emerging menace', *J. Hepatol.* **2012**, *56*, 1384–1391.
[3] B. C. Sun, M. Karin, 'Obesity, inflammation, and liver cancer', *J. Hepatol.* **2012**, *56*, 704–713.
[4] D. H. Palmer, 'Sorafenib in Advanced Hepatocellular Carcinoma', *N. Engl. J. Med.* **2008**, *359*, 2498–2498.
[5] S. F. Yang, G. H. Liu, 'Targeting the Ras/Raf/MEK/ERK pathway in hepatocellular carcinoma', *Oncol. Lett.* **2017**, *13*, 1041–1047.
[6] K. J. Schmitz, J. Wohlschlaeger, H. Lang, G. C. Sotiropoulos, M. Malago, K. Steveling, H. Reis, V. R. Cicinnati, K. W. Schmid, H. A. Baba, 'Activation of the ERK and AKT signalling pathway predicts poor prognosis in hepatocellular carcinoma and ERK activation in cancer tissue is associated with hepatitis C virus infection', *J. Hepatol.* **2008**, *48*, 83–90.
[7] J. H. Wright, E. Munar, D. R. Jameson, P. R. Andreassen, R. L. Margolis, R. Seger, E. G. Krebs, 'Mitogen-activated protein kinase activity is required for the G(2)/M transition of the cell cycle in mammalian fibroblasts', *Proc. Natl. Acad. Sci. USA* **1999**, *96*, 11335–11340.
[8] C. Hayne, G. Tzivion, Z. J. Luo, 'Raf-1/MEK/MAPK pathway is necessary for the G(2)/M transition induced by nocodazole', *J. Biol. Chem.* **2000**, *275*, 31876–31882.
[9] A. A. Reszka, R. Seger, C. D. Diltz, E. G. Krebs, E. H. Fischer, 'Association of Mitogen-Activated Protein-Kinase with the Microtubule Cytoskeleton', *Proc. Natl. Acad. Sci. USA* **1995**, *92*, 8881–8885.
[10] Q. Lu, K. S. Kosik, 'MAP kinase activity and the balance between cell-cell and cell-matrix interactions', *Mol. Biol. Cell* **1996**, *7*, 2678–2678.
[11] A. H. Ding, B. H. Chen, M. Fuortes, E. Blum, 'Association of mitogen-activated protein kinases with microtubules in mouse macrophages', *J. Exp. Med.* **1996**, *183*, 1899–1904.

[12] W. F. Tan, X. W. Zhang, M. H. Li, J. M. Yue, Y. Chen, L. P. Lin, J. Ding, 'Pseudolarix acid B inhibits angiogenesis by antagonizing the vascular endothelial growth factor-mediated anti-apoptotic effect', *Eur. J. Pharmacol.* **2004**, *499*, 219–228.
[13] J. A. Gollob, S. Wilhelm, C. Carter, S. L. Kelley, 'Role of Raf kinase in cancer: Therapeutic potential of targeting the Raf/MEK/ERK signal transduction pathway', *Semin. Oncol.* **2006**, *33*, 392–406.
[14] A. Kamal, A. Mallareddy, M. J. Ramaiah, S. N. C. V. L. Pushpavalli, P. Suresh, C. Kishor, J. N. S. R. C. Murty, N. S. Rao, S. Ghosh, A. Addlagatta, M. Pal-Bhadra, 'Synthesis and biological evaluation of combretastatin-amidobenzothiazole conjugates as potential anticancer agents', *Eur. J. Med. Chem.* **2012**, *56*, 166–178.
[15] M. A. Patil, M. S. Chua, K. H. Pan, R. Lin, C. J. Lih, S. T. Cheung, C. Ho, R. Li, S. T. Fan, S. N. Cohen, X. Chen, S. So, 'An integrated data analysis approach to characterize genes highly expressed in hepatocellular carcinoma', *Oncogene* **2005**, *24*, 3737–3747.
[16] C. Y. Tung, C. H. Jen, M. T. Hsu, H. W. Wang, C. H. Lin, 'A novel regulatory event-based gene set analysis method for exploring global functional changes in heterogeneous genomic data sets', *BMC Genomics* **2009**, *10*.
[17] Q. A. Zhou, A. K. K. Ching, W. K. C. Leung, C. Y. Y. Szeto, S. M. Ho, P. K. S. Chan, Y. F. Yuan, P. B. S. Lai, W. Yeo, N. Wong, 'Novel therapeutic potential in targeting microtubules by nanoparticle albumin-bound paclitaxel in hepatocellular carcinoma', *Int. J. Oncol.* **2011**, *38*, 721–731.
[18] H. H. Loong, W. Yeo, 'Microtubule-targeting agents in oncology and therapeutic potential in hepatocellular carcinoma', *OncoTargets Ther.* **2014**, *7*, 575–585.
[19] C. Kanthou, O. Greco, A. Stratford, I. Cook, R. Knight, O. Benzakour, G. Tozer, 'The tubulin-binding agent combretastatin A-4-phosphate arrests endothelial cells in mitosis and induces mitotic cell death', *Am. J. Pathol.* **2004**, *165*, 1401–1411.
[20] M. Rosner, K. Schipany, M. Hengstschlager, 'Merging high-quality biochemical fractionation with a refined flow cytometry approach to monitor nucleocytoplasmic protein expression throughout the unperturbed mammalian cell cycle', *Nat. Protoc.* **2013**, *8*, 602–626.
[21] C. D. Ley, M. R. Horsman, P. E. G. Kristjansen, 'Early Effects of Combretastatin-A4 Disodium Phosphate on Tumor Perfusion and Interstitial Fluid Pressure', *Neoplasia* **2007**, *9*, 108–112.
[22] S. T. Gutiérrez, S. D. Oltra, E. Falomir, J. Murga, M. Carda, J. A. Marco, 'Synthesis of combretastatin A-4 *O*-alkyl derivatives and evaluation of their cytotoxic, antiangiogenic and antitelomerase activity', *Bioorg. Med. Chem.* **2013**, *21*, 7267–7274.
[23] G. R. Pettit, S. B. Singh, E. Hamel, C. M. Lin, D. S. Alberts, D. Garia-Kendall, 'Isolation and structure of the strong cell growth and tubulin inhibitor combretastatin A4', *Experientia* **1989**, *45*, 205–211.
[24] E. Abma, S. Daminet, P. Smets, Y. Ni, H. de Rooster, 'Combretastatin A4-phosphate and its potential in veterinary oncology: a review', *Vet. Comp. Oncol.* **2017**, *15*, 184–193.
[25] K. Ohsumi, T. Hatanaka, K. Fujita, R. Nakagawa, Y. Fukuda, Y. Nihei, Y. Suga, Y. Morinaga, Y. Akiyama, T. Tsuji, 'Syntheses and antitumor activity of cis restricted combretastatins: 5-membered heterocyclic analogs', *Bioorg. Med. Chem. Lett.* **1998**, *8*, 3153–3158.
[26] T. Yang, Y. Wang, Z. Li, W. Dai, J. Yin, L. Liang, X. Ying, S. Zhou, J. Wang, X. Zhang, Q. Zhang, 'Targeted delivery of a combination therapy consisting of combretastatin A4 and low-dose doxorubicin against tumor neovasculature', *Nanomedicine* **2012**, *8*, 81–92.
[27] P. Nathan, M. Zweifel, A. R. Padhani, D. M. Koh, M. Ng, D. J. Collins, A. Harris, C. Carden, J. Smythe, N. Fisher, N. J. Taylor, J. J. Stirling, S. P. Lu, M. O. Leach, G. J. S. Rustin, I. Judson, 'Phase I Trial of Combretastatin A4 Phosphate (CA4P) in Combination with Bevacizumab in Patients with Advanced Cancer', *Clin. Cancer Res.* **2012**, *18*, OF1–OF12.
[28] M. Gao, D. Zhang, Q. Jin, C. Jiang, C. Wang, J. Li, F. Peng, D. Huang, J. Zhang, S. Song, 'Combretastatin-A4 phosphate improves the distribution and antitumor efficacy of albumin-bound paclitaxel in W256 breast carcinoma model', *Oncotarget* **2016**, *7*, 58133–58141.
[29] D. Kumar, S. Swapna, E. O. Johnson, K. Shah, 'An efficient synthesis and biological study of novel indolyl-1,3,4-oxadiazoles as potent anticancer agents', *Bioorg. Med. Chem. Lett.* **2009**, *19*, 4492.
[30] D. G. Zhao, J. J. Chen, Y.-R. Du, Y.-Y. Ma, Y.-X. Chen, K. Gao, B.-R. Hu, 'Synthesis and structure–activity relationships of *N*-methyl-5,6,7-trimethoxy indoles as novel antimitotic and vascular disrupting agents', *J. Med. Chem.* **2013**, *56*, 1467–1477.
[31] A. Brancale, R. Silvestri, 'Indole, a core nucleus for potent inhibitors of tubulin polymerization', *Med. Res. Rev.* **2007**, *27*, 209–238.
[32] G. La Regina, R. Bai, W. M. Rensen, E. Di Cesare, A. Coluccia, F. Piscitelli, V. Famiglini, A. Reggio, M. Nalli, S. Pelliccia, E. Da Pozzo, B. Costa, I. Granata, A. Porta, B. Maresca, A. Soriani, M. L. Iannitto, A. Santoni, J. Li, M. M. Cona, F. Chen, Y. Ni, A. Brancale, G. Dondio, S. Vultaggio, M. Varasi, C. Mercurio, C. Martini, E. Hamel, P. Lavia, E. Novellino, R. Silvestri, 'Toward highly potent cancer agents by modulating the C-2 group of the arylthioindole class of tubulin polymerization inhibitors', *J. Med. Chem.* **2013**, *56*, 123–149.
[33] P. V. S. Ramya, S. Angapelly, L. Guntuku, C. S. Digwal, B. N. Babu, V. G. M. Naidu, A. Kamal, 'Synthesis and biological evaluation of curcumin inspired indole analogs as tubulin polymerization inhibitors', *Eur. J. Med. Chem.* **2017**, *127*, 100–114.
[34] S. D. Guggilapu, G. Lalita, T. S. Reddy, S. K. Prajapti, A. Nagarsenkar, S. Ramu, U. R. Brahma, U. J. Lakshmi, G. M. N. Vegi, S. K. Bhargava, B. N. Babu, 'Synthesis of C5-tethered indolyl-3-glyoxylamide derivatives as tubulin polymerization inhibitors', *Eur. J. Med. Chem.* **2017**, *128*, 1–12.
[35] S. N. Baytas, N. Inceler, A. Yılmaz, A. Olgac, S. Menevse, E. Banoglu, E. Hamel, R. Bortolozzi, G. Viola, 'Synthesis, biological evaluation and molecular docking studies of *trans*-indole-3-acrylamide derivatives, a new class of tubulin polymerization inhibitors', *Bioorg. Med. Chem.* **2014**, *22*, 3096–3104.
[36] K. N. F. Shaw, A. McMillan, A. G. Gudmundson, M. D. Armstrong, 'Preparation and properties of β-3-indolyl compounds related to tryptophan metabolism', *J. Org. Chem.* **1958**, *23*, 1171–1178.

[37] A. Monks, S. D., P. Skehan, R. Shoemaker, K. Paull, D. Vistica, C. Hose, J. Langley, P. Cronise, A. Vaigro-Wolff, M. Gray-Goodrich, H. Campbell, J. Mayo, M. Boyd, 'Feasibility of a high-flux anticancer drug screen utilizing a diverse panel of human tumor cell lines in culture', *J. Natl. Cancer Inst.* **1991**, *83*, 757–766.
[38] A. Biosciences, 'Real-Time and Dynamic Monitoring of Cell Proliferation and Viability for Adherent Cells', 2013.
[39] I. Durmaz, E. B. Guven, T. Ersahin, M. Ozturk, I. Calis, R. Cetin-Atalay, 'Liver cancer cells are sensitive to Lanatoside C induced cell death independent of their PTEN status', *Phytomedicine* **2016**, *23*, 42–51.
[40] F. Buontempo, T. Ersahin, S. Missiroli, S. Senturk, D. Etro, M. Ozturk, S. Capitani, R. Cetin-Atalay, M. L. Neri, 'Inhibition of Akt signaling in hepatoma cells induces apoptotic cell death independent of Akt activation status', *Invest. New Drugs* **2011**, *29*, 1303–1313.
[41] M. M. Hawash, D. C. Kahraman, F. Eren, R. Cetin-Atalay, S. N. Baytas, 'Synthesis and biological evaluation of novel pyrazolic chalcone derivatives as novel hepatocellular carcinoma therapeutics', *Eur. J. Med. Chem.* **2017**, *129*, 12–26.

Received December 17, 2020
Accepted March 12, 2021

